Accepted Manuscript

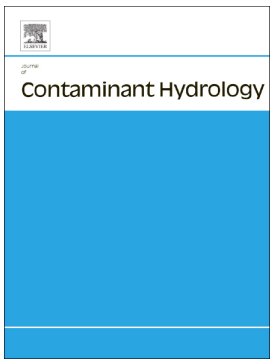

The role of intra-NAPL diffusion on mass transfer from MGP residuals

Saeid Shafieiyoun, Neil R. Thomson

PII: S0169-7722(17)30303-0
DOI: doi:10.1016/j.jconhyd.2018.04.002
Reference: CONHYD 3389

To appear in: *Journal of Contaminant Hydrology*

Received date: 26 September 2017
Revised date: 15 March 2018
Accepted date: 20 April 2018

Please cite this article as: Saeid Shafieiyoun, Neil R. Thomson , The role of intra-NAPL diffusion on mass transfer from MGP residuals. The address for the corresponding author was captured as affiliation for all authors. Please check if appropriate. Conhyd(2018), doi:10.1016/j.jconhyd.2018.04.002

The Role of Intra-NAPL Diffusion on Mass Transfer from MGP Residuals

Saeid Shafieiyoun* and Neil R. Thomson
Department of Civil and Environmental Engineering
University of Waterloo
200 University Avenue West
Waterloo, Ontario, Canada
N2L 3G1
(*corresponding author; E-mail:s5shafie@uwaterloo.ca)

ABSTRACT

An experimental and computational study was performed to investigate the role of multi-component intra-NAPL diffusion on NAPL-water mass transfer. Molecular weight and the NAPL component concentrations were determined to be the most important parameters affecting intra-NAPL diffusion coefficients. Four NAPLs with different viscosities but the same quantified mass were simulated. For a spherical NAPL body, a combination of NAPL properties and interphase mass transfer rate can result in internal diffusion limitations. When the main intra-NAPL diffusion coefficients are in the range of self-diffusion coefficients (10^{-5} to 10^{-6} cm^2/s), dissolution is not limited by internal diffusion except for high mass transfer rate coefficients (>180 cm/day). For a complex and relatively high viscous NAPL (>50 g/(cm s)), smaller intra-NAPL diffusion coefficients (<10^{-8}) are expected and even low mass transfer rate coefficients (~6 cm/day) can result in diffusion-limited dissolution.

KEY WORDS

Intra-NAPL diffusion, intra-NAPL concentration gradient, rate-limited mass transfer, MGP residuals

1.0 INTRODUCTION

The remediation of soil and groundwater contaminated with multi-component non-aqueous phase liquids (NAPLs) such as crude oil, creosote, or coal tars from former manufactured gas plants (MGP) is associated with a number of challenges (Birak & Miller, 2009). One of the primary factors that restricts the performance of remedial technologies for multi-component NAPLs is the extent and rate of NAPL dissolution (Luthy et al., 1994). Mass transfer kinetics at the NAPL-water interface is usually described by a stagnant film model (Miller et al., 1990) wherein the dissolution of organic components from the NAPL into the aqueous phase is comprised of several mass transfer steps (Seagren et al., 1993; Heyse et al., 2002;). The first step involves the diffusion of organic molecules towards the NAPL-water interface boundary layer, while the second step is diffusion through a rigid or emulsion interface between the water and NAPL. This interface is formed due to depletion of more soluble compounds at the NAPL boundary, and can completely separate the bulk-aqueous and bulk-NAPL phases by a film composed of either an aqueous film, or an interfacial organic film, or both (Peters et al., 2000; Wehrer et al., 2013a). In the third step, the organic molecules will dissolve in the bulk-aqueous phase after passing through the aqueous film. Each of these mass transfer steps can be limiting since they act in series, and the one with the highest resistance will control the overall dissolution of an organic compound into the aqueous phase (Ortiz et al., 1999; Wehrer et al., 2013a).

A substantial body of field and laboratory data (e.g., Hunt et al., 1988; Mercer & Cohen, 1990; Powers et al., 1992; Seagren et al., 1999; Mobile et al., 2016) has shown that the concentration of organic compounds in groundwater is usually less than their corresponding equilibrium concentration at various observation scales. This implies that NAPL architecture, flow bypassing, low residual saturation (Powers et al., 1998; Soga et al., 2004), and diffusional transport limitations (Luthy et al., 1993; Ortiz et al., 1999; Wehrer et al., 2013a; Lekmine et al., 2014) can impact dissolution. Consequently, dissolution of organic components is usually modeled as a rate-limited process with diffusion governing the mass transfer through the NAPL-water interface.

Due to thermodynamics, the presence of more than one component within a multi-component NAPL may restrict intra-NAPL diffusion (Cussler, 1997; Ortiz et al., 1999). This occurs since the diffusion of each component is related to its own concentration gradient as well as the concentration gradients of the other components present in the organic mixture (Cussler, 1997; Zielinski & Hanley, 1999). For example, Mukherji et al. (1997) investigated the aqueous equilibrium concentrations of a continuously-stirred mixture of four synthetic dense NAPLs (DNAPLs) composed of structurally similar components that were in direct interaction with an aqueous phase. The results demonstrated that experimental equilibrium concentrations were within a factor of two compared to values predicted by modified Raoult's law (Lee et al., 1992) for an ideal mixture indicating that non-ideal interactions were not observed between components. However, the assumption of a well-mixed ideal mixture with structurally similar components is not always applicable in most subsurface systems (Khachikian & Harmon, 2000). Miller et al. (1985) reported that non-ideal behaviour will escalate when the molecular size of components are larger than octanol, and Banerjee et al. (1984) indicated that the presence of dissimilar molecules in organic mixtures resulted in deviation from ideal behaviour. By extension, it is expected that the effects of intra-NAPL diffusion will be more significant in multi-component NAPLs such as MGP residuals which are composed of hundreds to thousands of structurally dissimilar organic components (Luthy et al., 1993; Brown et al., 1999; Birak & Miller, 2009). When multi-component NAPLs are exposed to groundwater, the more soluble components will dissolve leaving the less soluble components at the interface (Liu et al., 2009; Peters et al., 2000). Diffusional resistance within a multi-component NAPL may then limit the movement of organic molecules toward the interface (Ortiz et al., 1999), and hence a new emulsion-like and high viscous interfacial film or a skin can be formed on the NAPL surface. This phenomenon is called weathering or aging, and affects diffusion across the NAPL-water interface, and consequently the dissolution of organic compounds will be reduced (Liu et al., 2009; Wehrer et al., 2013a,b).

Previous research indicates that coal tar, creosote, and crude oil weathering effects have been experimentally observed and attributed to either NAPL composition or inter-molecular interactions at the NAPL-water interface (Luthy et al., 1993; Nelson et al., 1996; Mahjoub et al., 2000; Alshafie & Ghoshal, 2004; Ghoshal et al., 2004).

Luthy et al. (1993) observed the formation of a semi-rigid, skin-like layer at the interface of a coal tar drop suspended in water after three days, and this layer led to reduced NAPL-water mass transfer and a disequilibrium condition after seven days. Ghoshal et al. (2004) reported that a skin layer at a crude oil-water interface reduced the mass transfer coefficient by up to 80 percent after 35 days. It has been suggested that crude oil-water interfacial films are mostly comprised of asphaltenes and polar resins (Strassner, 1968; Jada & Salou, 2002; Ghoshal et al., 2004; Varadaraj & Brons, 2012). Nelson et al. (1996) hypothesized that inter-molecular interactions at a coal tar-water interface resulted in the formation of a semi-gelatinous film. Barranco and Dawson (1999) reported that even a small fraction of asphaltenic components in coal tar can affect interfacial properties. Barranco and Dawson (1999) also indicated that film formation at a coal tar-water interface occurred under acidic to neutral pH rather than alkaline conditions. Finally, Powers et al. (1996), and Brown and Neustadter (1980) observed that film formation at a crude oil-water interface affected mineral wettability.

Surprisingly, the role of intra-NAPL diffusion on the dissolution of organic components from NAPL sources has received little attention. Holman and Javandel (1996) employed a simplified two-dimensional intra-NAPL diffusive flux expression with a constant diffusion coefficient to represent the dissolution from a light NAPL (LNAPL) pool. In this model the dissolution of each organic component was independent of others, and the local equilibrium assumption was considered at the LNAPL-water interface. Brahma and Harmon (2003) assessed multi-component diffusion within two ternary organic mixtures using hydrodynamic diffusion theory (Hartley & Crank, 1949) and the Kett and Anderson model (1969a). While this work provides valuable insight, the peer-reviewed literature in this area has investigated organic mixtures comprised of only a few components. In addition, concentration profiles and diffusion limitations within a NAPL body have not been mathematically simulated.

The objective of this study was to determine the role of multi-component intra-NAPL diffusion on NAPL-water mass transfer, interfacial depletion of the more soluble compounds, and to identify some of the conditions where this process needs to be considered. To support this evaluation, a numerical model was developed to simulate mass discharge and intra-NAPL concentration gradients. A series of static

experiments were conducted using coal tar collected from a former MGP site to capture multi-component diffusion-limited mass transfer behavior. These experiments were designed to generate relevant model parameters (e.g., mass transfer rate coefficients, equilibrium concentrations, activity coefficients, and NAPL characteristics) for simulation purposes.

1.1 INTRA-NAPL DIFFUSION THEORY

Diffusive flux within a multi-component NAPL depends on the molecular interactions and relative abundance of components present in the system (Weber & DiGiano, 1995; Lekmine et al., 2014). According to Fick's law, a multi-component diffusive flux can be represented as (Cussler, 1997):

$$-J_i = \sum_{j=1}^{n-1} D_{ij} \nabla C_j \quad (1)$$

where n is the total number of components with component n arbitrarily chosen as the solvent, and D_{ij} represents multi-component diffusion coefficients employed to approximate diffusivity within a system of n components. The array, D_{ij}, includes $(n-1)^2$ diffusion coefficients where the diagonal terms, D_{ii}, represent the effects of the concentration gradient of component i on its own flux, and the off-diagonal or cross-coefficients, D_{ij}, reflect the effects of the concentration gradients of other components present in the mixture on the flux of component i (Zielinski & Hanley, 1999). The off-diagonal diffusion coefficients can be positive or negative indicating that diffusion of one component can be enhanced or hindered by other components present in the organic mixture (Brahma & Harmon, 2003).

Few theoretical models have been developed to predict the diffusion coefficients in multi-component mixtures (Kett & Anderson, 1969a; Cussler, 1997; Zielinski & Hanley, 1999; Leahy-Dios & Firoozabadi, 2007). In this study, the intra-NAPL diffusion coefficients were estimated by the model developed by Kett and Anderson (1969a). In this model the hydrodynamic theory of Hartley and Crank (1949) was applied to the multi-component Fickian diffusion process in non-associating, non-electrolyte solutions of any number of components. The generalized expressions to estimate multi-component diffusion coefficients in non-associating solutions were

developed (Kett & Anderson, 1969a) and validated by experimental evidence (Kett & Anderson, 1969b) using two non-associating ternary systems (dodecane-hexadecane-hexane, and toluene-chlorobenzene-bromobenzene).

According to hydrodynamic theory (Hartley & Crank, 1949), the diffusive flux consists of two different types of motion: intrinsic diffusion (molecular motion), and bulk motion of the medium. Intrinsic diffusion is related to the energy of each molecule to move compared to the surrounding molecules, and bulk motion results from the flow of other components present in the mixture to compensate the accumulation of mass in one region. Kett and Anderson (1969a) described the intrinsic diffusion flux by equating the driving and resisting forces imparted on a diffusing molecule as:

$$J_i = -\frac{C_i}{\sigma_i \eta}\frac{\partial \mu_i}{\partial x} \tag{2}$$

where J_i is the flux of component i relative to the medium resulting from intrinsic diffusion, C_i is the concentration in the NAPL, $\frac{\partial \mu_i}{\partial x}$ is the chemical potential gradient, η is mixture viscosity, and σ_i is a proportionality coefficient called the friction factor representing the effects of the shape and size of the diffusing molecule. At constant pressure and temperature, the chemical potential gradient in Eq.2 can be related to the concentration gradient. Consequently, the diffusive flux (Eq.2) is equivalent to the Fick's law, and the general expressions for the diffusion coefficients (D_{ij}) can be derived. While Kett and Anderson (1969b) derived the D_{ij} expressions for a ternary system, in this study the general form of D_{ij} for a system of n components was derived to estimate the intra-NAPL diffusion coefficients within a NAPL (see Supplementary Material (SM) for details). The diagonal terms (D_{ii}) can be represented as:

$$D_{ii} = \frac{RTC_i}{\eta}\left\{\left(\frac{1-V_iC_i}{\sigma_i}+\frac{V_nC_i}{\sigma_n}\right)\left[\left(\frac{\partial ln\gamma_i}{\partial C_i}\right)+\frac{1}{C_i}-\frac{1}{C_T}\left(1-\frac{V_i}{V_n}\right)\right] + \sum_{k=1,(k\neq i)}^{n-1} C_k\left(\frac{V_n}{\sigma_n}-\frac{V_k}{\sigma_k}\right)\left[\left(\frac{\partial ln\gamma_k}{\partial C_i}\right)-\frac{1}{C_T}\left(1-\frac{V_i}{V_n}\right)\right]\right\} \tag{3a}$$

and the off-diagonal coefficients ($D_{ij,i\neq j}$) can be written as:

$$D_{ij} = \frac{RTC_i}{\eta}\left\{\left(\frac{1-V_iC_i}{\sigma_i}+\frac{V_nC_i}{\sigma_n}\right)\left[\left(\frac{\partial ln\gamma_i}{\partial C_j}\right)-\frac{1}{C_T}\left(1-\frac{V_j}{V_n}\right)\right]+C_j\left(\frac{V_n}{\sigma_n}-\frac{V_j}{\sigma_j}\right)\left[\left(\frac{\partial ln\gamma_j}{\partial C_j}\right)+\frac{1}{C_j}-\frac{1}{C_T}\left(1-\frac{V_j}{V_n}\right)\right]\right.$$

$$\left.+\sum_{k=1,(k\neq i,j)}^{n-1} C_k\left(\frac{V_n}{\sigma_n}-\frac{V_k}{\sigma_k}\right)\left[\left(\frac{\partial ln\gamma_k}{\partial C_j}\right)-\frac{1}{C_T}\left(1-\frac{V_j}{V_n}\right)\right]\right\}$$

(3b)

whereC_T is the sum of molar concentrations of components present in the mixture, γ is the activity coefficient, V_j is the molar volume, R is the universal gas constant, and T is the absolute temperature. The derivative of the activity coefficient with respect to the concentration of each component ($\frac{\partial \ln\gamma}{\partial C_i}$), can be estimated using the activity coefficient data by assuming that the concentrations of other components present in the system are constant. Kett and Anderson (1969a) suggested that if the self-diffusion (D_i) and infinite dilution diffusion coefficients (D_{ij}^o) for each component are available, the local friction factor can be estimated as:

$$\sigma_i = RT\left(\frac{X_i}{D_i\eta_i}+\sum_{j=1,j\neq i}^{n}\frac{X_j}{D_{ij}^o\eta_j}\right) \quad (4)$$

where X_i is the mole fraction of each component within the NAPL mixture, and η_i is the viscosity of each pure component. Self-diffusion represents the diffusion process of each component in its own pure state and is defined by Albright and Miller (1965) as “the special case of intra-diffusion for systems that contain no other components than two isotopic forms of a chemical species”. Infinite dilution diffusion represents the interactions between two components in a mixture and was defined by Kett and Anderson (1969a) as “the mutual-diffusion coefficient of the *i j* binary at infinite dilution of *i* ”.

2.0 EXPERIMENTAL INVESTIGATION

2.1 MATERIALS AND METHODS

To examine the direct interaction between a multi-component NAPL and an aqueous phase, and to investigate diffusion-limited mass transfer and dissolution behavior of organic components, a series of static experiments using 10 mL (nominal) Pyrex graduated conical centrifuge vials was performed.

The MGP residuals used in this study were obtained from the former West Florida Natural Gas Company Site located in Ocala, Florida. From the late 1890s until about 1953, water gas or carbureted water gas was manufactured at this location by the "Lowe" carbonization process or destructive distillation of bituminous coal and coke. According to Brown's Directory, gas production was ~48 x 10^3 m^3/yr in 1900 and steadily increased to 900 x 10^3 m^3/yr by 1950. In 1952, manufacturing stopped at the plant and the facility converted to the sale of butane-propane-air. Residues from the MGP process, including tars and oily wastewaters, were deposited in the area of the former gas plant facilities during operations. There was an historic coal tar pit or area where residual tars were stored prior to sale for off-site use as roofing materials. The MGP residual received was obtained from a NAPL collection well screened from 24 to 27 m below ground surface in weathered limestone, and was a non-homogeneous mixture composed of a LNAPL and DNAPL portion with minor sediment. For the purpose of this experiment, our focus was on the DNAPL portion. Thus, 10 mL of the MGP residual was mixed with 10 mL Milli-Q water in a 40 mL vial and centrifuged at 10,000 rpm for 15 min. The DNAPL portion was collected after centrifuging and again mixed with water and centrifuged. This process was repeated multiple times to separate a sufficient mass of DNAPL which was then used. The final DNAPL volume was assumed to be a homogeneous mixture, and the viscosity was determined to be 1.22 g/(cm s) using a dilution viscometer (Cannon-Ubbelhode) and the density of NAPL was determined to be 1.08 g/mL. Table 1 provides a summary of the most abundant and soluble components detected within the DNAPL portion along with some associated properties. The identified 19 components account for ~40 % of the total NAPL mass. The remainder of the NAPL mass was unidentified and assumed to be composed of higher molecular weight and lower soluble components.

Each 10 mL conical vial was partially filled with Milli-Q water and then 0.1 mL of the homogenised NAPL was gradually injected into the bottom of each vial through the water using a 100 µL glass syringe (Hamilton, Sigma Aldrich). The vials were then completely filled with Milli-Q water (total volume of water was 11.2 mL). The NAPL-water surface area was ~0.10 cm^2. A total of 18 vials were constructed and left in the dark at an ambient temperature of 20 ^oC. The vials were not disturbed to ensure that NAPL-water mass transfer was limited only to diffusional transport of organic components. Duplicate reactors were sacrificed at each time increment (e.g., 2, 7, 12, 15, 22, 28, 36, 49, and 61 days). The aqueous solution was removed by a 10 mL glass syringe (Hamilton, Sigma Aldrich,) mixed, then centrifuged for 15 minutes at 6000 rpm to separate possible undissolved DNAPL. The concentration of organic compounds (Table 1) present in the aqueous sample along with the solution pH (Orion pH meter, model 290A) was determined. Since the aqueous phase was mixed and centrifuged, the experimental aqueous concentrations represent average concentrations above the NAPL as indicated by the total dissolved mass divided by the total volume of water in each reactor.

For analysis of the organic components in the aqueous phase, a 5 mL sample was mixed with 14 mL of water in a 20 mL vial. This was followed immediately by the addition of 1.0 mL of methylene chloride (containing internal standards metafluoro-toluene (MFT) and fluoro-biphenyl (FBP) at 25 mg/L). The vial was quickly resealed and agitated on its side at 350 rpm on a platform shaker for 20 min. After shaking, the vial was inverted and the phases were allowed to separate for 30 min. Approximately 0.7 mL of the dichloromethane phase was removed from the inverted vial with a gas tight glass syringe through the Teflon septum. The solvent was placed in a 2.0 mL Teflon sealed autosampler vial for injection into the gas chromatograph (GC). For the analysis of the DNAPL portion, a sub-sample was added directly to methylene chloride and transferred to a 2.0 mL autosampler vial and crimp sealed with a Teflon cap. All NAPL and aqueous samples were analyzed using a HP 5890 capillary GC, a HP7673A autosampler, and a flame ionization detector. Three (3) mL of methylene chloride was injected in splitless mode (purge on 0.5 min, purge off 10 min) onto a 0.25 mm x 30 m length, DB5 capillary column with a stationary phase film thickness of 0.25 µm. The helium column flow rate was 2.0 mL/min with a make-up gas flow rate of 30 mL/min. The injection temperature was 275 ^oC, detector

temperature was 325 ^{o}C and initial column oven temperature was 35 ^{o}C held for 0.5 min, then ramped up at 15 ^{o}C/min to a final temperature of 250 ^{o}C and held for 2 min. A GC run time was 16 min. Data integration was completed with a SRI Model 302 Peak Simple chromatography data system. The method detection limit (MDL) was 5 mg/kg for NAPL samples and for aqueous samples are reported in Table 1.

2.2 RESULTS AND DISCUSSION

A total of nine components were detected in the aqueous phase including BTEX (benzene, toluene, ethylbenzene, and xylene), trimethylbenzene, and four polycyclic aromatic hydrocarbons (PAHs) (naphthalene, 1-methylnaphthalene, 2-methylnaphthalene, and acenaphthene). The other components listed in Table 1 were < MDL. The average pH value of the aqueous phase was 5.3 at the start of the experiment and decreased gradually to 4.5 by Day 61 likely due to the dissolution of organic acids. No physical changes (i.e., color, temperature, precipitate formation) were observed. The diffusion-limited dissolution of this MGP residual in water manifested in these static experiments as an initial rapid increase of dissolved phase concentrations from Day 2 to Day 10 followed by minor fluctuations until Day 61 (Figure 1). Except for naphthalene, xylene and ethylbenzene, the detected components appear to reach an equilibrium concentration by Day 61 (Table 2).

Lee et al. (1992) indicated that the aqueous equilibrium concentration of PAHs within coal tars can be estimated by employing a modified form of Raoult's law given by:

$$C_{eq,i}^{w} = X_i^N \gamma_i^N \frac{S_i}{(f_i^s / f_i^l)} \tag{5}$$

where $C_{eq,i}^{w}$ is aqueous equilibrium concentration of each component, N and w superscripts refer to NAPL and water phase respectively, S_i is the aqueous solubility, and f_i^s and f_i^l are fugacities in the pure solid and pure liquid states respectively (Table 1). Naphthalene and benzene due to the high mole fraction and solubility values, respectively, have the highest aqueous phase concentrations. While ethylbenzene, xylene, toluene, and trimethylbenzene have a higher solubility compared to naphthalene, they have lower equilibrium concentrations due to lower mole fractions and higher fugacity ratios. Toluene has the lowest aqueous

concentration which is proportional to its low mole fraction within the NAPL. 1-methylnaphthalene and 2-methylnaphthalene show similar behaviour and reach an equilibrium concentration in < 30 days.

Since the experimental aqueous concentrations represent the average concentrations, the aqueous phase mass balance using the stagnant film model for each organic component can be written as (Miller et al., 1990):

$$\frac{dc_i^w}{dt} = K_i(C_{eq,i}^w - C_i^w) \tag{6}$$

where C_i^w is aqueous concentration, t is time, K_i is lumped mass transfer rate coefficient (1/T), and $C_{eq,i}^w$ is the aqueous equilibrium concentration. To determine the lumped mass transfer rate coefficient for each component, Eq.6 can be solved analytically with the initial condition specified as an aqueous concentration of zero at $t = 0$, to yield:

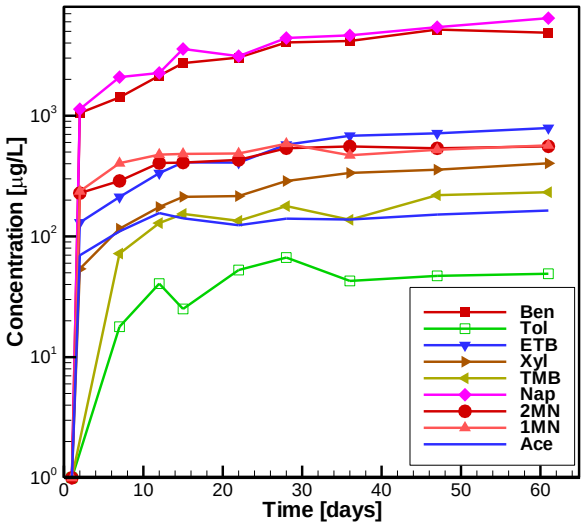

Figure 1: Temporal concentration profiles of the nine detected components observed in the bulk solution for the static diffusion experiments.

$$\ln\left(1-\frac{C_i^w}{C_{eq,i}^w}\right)=-K_i t \quad (7)$$

Eq.7 was applied to the experimental data (Figure 1) and the lumped mass transfer rate coefficient for each component was determined using linear regression. The resulting values ranged from 0.036 to 0.1 /day. For naphthalene, xylene and ethylbenzene, the equilibrium concentrations were also estimated using a least squares analysis and presented along with the estimated lumped mass transfer data in Table 2. The lumped mass transfer rate coefficients were multiplied by the experimental aqueous volume (11.2 mL) and divided by the NAPL-water surface area (0.1 cm^2) to estimate mass transfer rate coefficients which varied from 4 to 11.2 cm/day with 1-methylnaphthalene and 2-methylnaphthalene having the highest values (~11.2 cm/day), and toluene and naphthalene the lowest values (4.0 cm/day).

Mukherji et al. (1997) observed that higher molecular weight compounds have larger mass transfer rate coefficients. Wehrer et al. (2013a) placed fresh and aged NAPLs into dialysis tubing and, in contrast to Mukherji et al. (1997), did not mix the NAPL. They determined an inverse dependency between molecular weight and intra-NAPL

diffusion coefficients by fitting a spherical diffusion model to experimental NAPL concentration data implying that higher molecular weight and size act as a resisting force for diffusional transport. Wehrer et al.(2013a) also reported that the inverse dependency between diffusion coefficients and molecular weight was much less pronounced for aged MGP residuals compared to fresh MGP tars. Similarly, for the MGP residual used in this study, no overall trend was observed between molecular weight and mass transfer rate coefficient (Figure 2). Rather an inverse dependency of the mass transfer rate coefficient on molecular weight is evident for the BTEX components. A similar but separate trend is apparent between the mass transfer rate coefficients and the molecular weight for the PAHs (1-methylnaphthalene, 2-methylnaphthalene and acenaphthene) except for naphthalene (MW = 128.2 g/mol) which has a smaller *K* compared to 1-methylnaphthalene and 2-methylnaphthalene (MW = 142 g/mol). The distinct inverse dependency of mass transfer rate coefficient on molecular weight for BTEX and PAHs suggests that BTEX and PAHs have different mass transfer behavior.

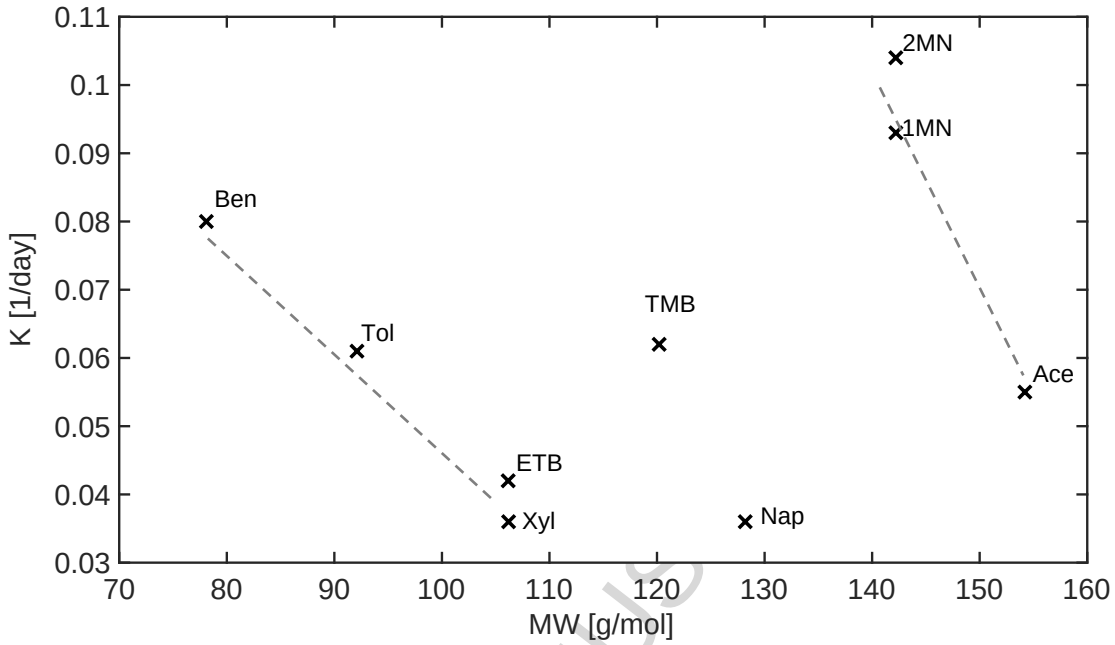

Figure 2: Lumped mass transfer rate coefficient (1/day) for each detectable component in the aqueous phase versus molecular weight (MW). The dashed lines represent observed trends for BTEX and three PAH compounds.

3.0 MULTI-COMPONENT INTRA-NAPL DIFFUSION MODEL

3.1 MODEL DESCRIPTION

To explore the role of intra-NAPL diffusion on the NAPL-water mass transfer, a temporal-spatial diffusion-based mathematical model was developed. For the purpose of this evaluation, an isolated initially homogeneous spherical NAPL blob with the total surface area available for mass transfer was considered to be suspended in a volume of water (Figure 3). The mass balance for each component within a spherical NAPL blob can be written as (Bird et al., 2002):

$$\frac{\partial \mathrm{C_i}}{\partial \mathrm{t}} = \frac{1}{r^2}\,\frac{\partial}{\partial \mathrm{r}}\left(r^2 \sum_{j=1}^{n-1} \mathrm{D_{ij}}\,\frac{\partial \mathrm{C_j}}{\partial \mathrm{r}}\right) \tag{8}$$

where *r* is the radial coordinate and changes in the mixture density are negligible. If the volume of water surrounding the spherical NAPL blob is small, the system will reach to an equilibrium condition quickly, while if the volume of water is large, a longer period of time is required to reach equilibrium condition and thus the NAPL blob may be depleted.

Eq.8 was subjected to the boundary conditions of $\frac{\partial C}{\partial r} = 0$ at the centre of the NAPL sphere, and the flux (J_i) at the external sphere NAPL-water boundary was equated to the first-order mass transfer expression (Miller et al., 1990; Weber & DiGiano, 1995) as given by:

$$J_i = K(C_{eq,i}^{w} - C_i^{w}) \tag{9}$$

where K is the mass transfer rate coefficient (L/T). The aqueous equilibrium concentration for each component ($C_{eq,i}^{w}$) was estimated by using the modified form of Raoult's law (Eq.5). To account for the film transfer resistance and compositional changes at the NAPL, the mole fractions in Eq.5 were based on the component concentrations at the external NAPL sphere boundary. Activity coefficients (γ_i) were calculated using the universal Quasi-chemical functional group activity coefficient (UNIFAC) (Poling et al., 2001).

Details of the numerical solution employed to solve Eqs 8 and 9 are provided in the

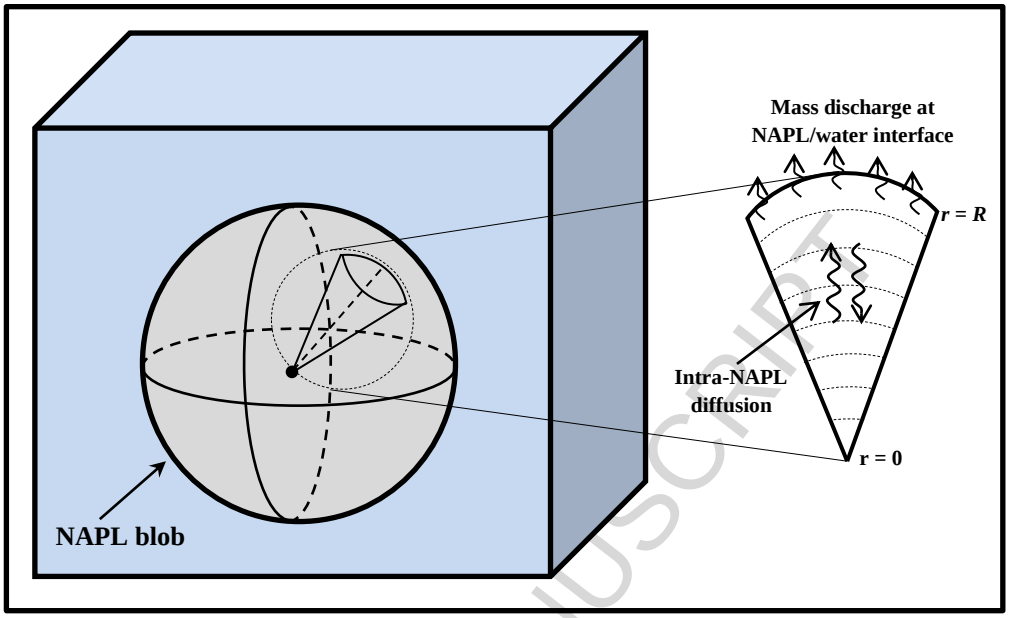

SM section.

Figure 3: Schematic of the physical system simulated consisting of a spherical NAPL blob suspended in a volume of water. Also shown is the numerical representation associated with Eq. 8.

3.2 MODEL PARAMETRIZATION AND INVESTIGATED SCENARIOS

The results from the experimental investigation indicated that diffusion-controlled dissolution behavior under static conditions occurred. In addition, the data from the static experiments were used to derive mass transfer rate coefficients, and aqueous equilibrium concentrations for the nine detected components associated with the former MGP NAPL employed. It was not our intent here to simulate the experimental conditions, but rather to use the data set assembled to inform model parameters so that representative physical and chemical properties are used.

For the initial condition for Eq.8, a 0.5 g homogenous spherical NAPL blob (radius of ~ 0.48 cm) surrounded by an aqueous phase was specified, and the initial concentration of organic components were assigned to be identical to the former MGP NAPL employed in the static experiments (Table 1) which contained 19 representative organic compounds (40% of the NAPL mass). The remainder of NAPL mass was considered to be comprised of an unresolved or bulk portion composed of higher molecular weight and lower soluble components and assigned nominal values (see Table 1). Since the focus of this study was to explore intra-NAPL compositional changes, 50 L of water was assumed to surround the NAPL blob. This volume was chosen so that the dissolved phase concentrations did not reach equilibrium over the simulation period allowing compositional changes within the NAPL to be observed.

For the estimation of intra-NAPL diffusion coefficients (D_{ij}) using Eq.3, a temperature of 20 °C was assumed and the mixture viscosity was estimated using the Grunberg and Nissan relationship (Grunberg & Nissan, 1949; Poling et al., 2001):

$$\ln(\eta) = \sum_{i=1}^{n} X_i \ln\eta_i + 0.5 \sum_{i=1}^{n} \sum_{j=1}^{n} X_i X_j G_{ij} \quad (10)$$

where G_{ij} is an interaction parameter which is a function of temperature as well as components i and j and estimated by a group contribution technique ($G_{ii} = 0$). The viscosity of each compound (η_i) was obtained from the literature (Lide et al., 1999),

or estimated by using the Orrick and Erbar method (Poling et al., 2001) with an average deviation of 15% as given by:

$$\ln\left(\frac{\eta_i}{100\,\rho_i MW}\right) = A + \frac{B}{T} \tag{11}$$

where MW is molecular weight (g/mol), T is absolute temperature, A and B are estimated by a group contribution technique, and the units for viscosity and density are g/(cm s), and g/cm^3 respectively. Table 1 summarizes the molecular weight, viscosity, and density values of each component. For the bulk portion, the molecular weight was assumed, and the density was assigned a value of 1.14 g/cm^3.

To estimate the friction factors (Eq.4), the self and infinite dilution diffusion coefficients for PAHs with a fugacity ratio less than unity were estimated similar to the other components which are liquid at ambient temperature. This approach is plausible since PAHs with a fugacity ratio less than unity can exist as liquid due to melting point depression within multi-component mixtures (Peters et al. 1997). The infinite dilution diffusion coefficients (D_{ij}^o) were determined using a modified form of the Tyn and Calus relationship (Poling et al., 2001), and the self-diffusion values (D_i) were calculated using the Houghton's Cubic Cell model (Houghton, 1964) as given by:

$$D_{ij}^o = 8.93 \times 10^{-10} \left(\frac{\bar{V}_{j,b}^{0.267}}{\bar{V}_{i,b}^{0.433}}\right) \frac{T}{\eta_j} \left(\frac{\tau_j}{\tau_i}\right)^{0.15} \tag{12}$$

$$D_i = \frac{RT\rho_i}{6\eta_i M_i} \left(\frac{V_i}{N}\right)^{\frac{2}{3}} \tag{13}$$

where D_i and D_{ij}^o have units of cm^2/s, viscosity (η) has units of g/(cm s), density has units of g/cm^3, M is molecular weight (g/mol), R is the universal gas constant (8.314x10^7 (g cm^2)/(s^2 K mol)), N is Avogadro's number (6.022x10^{23} 1/mol), τ is surface tension at boiling temperature (g/s^2), V is molar volume (cm^3/mol) which can be estimated using density and molecular weight data (MW/ρ) (Table 1), and $\bar{V}_b$ is molar volume at boiling temperature (cm^3/mol) and was estimated using the Schroeder relationship (Poling et al., 2001) (Table 1). The Schroeder relationship is an additive method which accounts for the number of atoms of carbon (C), hydrogen

(H), oxygen (O), nitrogen (N), halogens (Cl, F, I), sulfur (S), and also the number of carbon double bonds (DB), and triple bonds (TB):

$$\bar{V}_b = 7(N_C + N_H + N_O + N_N + N_{DB} + 2N_{TB}) + 31.5N_{Br} + 24.5N_{Cl} + 10.5N_F + 38.5N_I + 21N_S - 7 \quad (14)$$

where the last term is included only if the component has one or more rings. This method is accurate and except for highly associated liquids, gives an average error of 3-4% (Poling et al., 2001). The surface tension ratio (τ_j/τ_i) in Eq.12 was assumed to equal one (Poling et al., 2001). All of the estimated self and infinite dilution diffusion values are presented in Table SM.2. D_i and D_{ij}^o values for BTEX and methylethylbenzene(s) are in the range of 10^{-5} (cm^2/s), and for PAHs are in the range of 10^{-6} (cm^2/s). Since naphthalene is the most predominant component, D_i and $\bar{V}_b$ values for bulk portion of the NAPL were assumed to be similar to naphthalene.

NAPL viscosity can significantly affect mass transfer and intra-NAPL diffusional behavior. Ortiz et al. (1999) indicated that control on mass transfer can change from aqueous to NAPL resistance for high viscous NAPLs. Birak and Miller (2009) reported that the viscosity of MGP residuals comprised of coal, water-gas, and oil gas tars can range from 0.091 to 6600 g/(cm s). In a study by Wehrer et al. (2013a) the viscosity of various fresh and aged coal tars at 20 ^oC varied from 0.05 to 2.3 g/(cm s). The viscosity of the former MGP NAPL used in the experiment investigation (Section 2) was 1.22 g/(cm s) which lies in the middle of the viscosity range reported by Wehrer et al. (2013a). To explore the effects of NAPL viscosity on internal diffusion and mass transfer processes, four NAPL mixture viscosities were investigated: low (0.12 g/(cm s)), medium (1.22 g/(cm s) representative of the NAPL used in the experiment investigation, high (50 g/(cm s)), and very-high (400 g/(cm s)). To generate these mixture viscosities, the viscosity of the bulk portion for the low, medium, high, and very-high viscous NAPLs was assumed to be 0.3, 8, 600, and 5000 g/(cm s), respectively.

Experimental mass transfer rate coefficients (K) determined in Section 2.2 (Table 2) were considered for the 9 components detected in the aqueous phase (Figure 1). For the remaining components, a single mass transfer rate coefficient (Eq.9) was used and assigned a value that represented the aqueous experimental data for the nine detected components (Figure 1). The best-fit lumped mass transfer rate

coefficient using a least-squares analysis framework was estimated to be 0.056 /day. This value was converted to a mass transfer rate coefficient (K) of 6.16 cm/day using the experimental aqueous volume (11.2 mL) and NAPL-water surface area (~0.1 cm^2). Note that experimental aqueous concentrations were average values representative of the entire aqueous volume of the reactor, and the *K* values were determined by assuming a stagnant film boundary and the average aqueous concentrations (Eq.7). Hence, for simulation purposes the average concentrations (C_i^w) were used and mass flux from the spherical NAPL body was equated to the first-order mass transfer expression (Eq.9). Diffusion in the water surrounding the NAPL blob was ignoring since our interest in this investigation was intra-NAPL diffusion. The magnitude of the molecular diffusion coefficient in free water is ~10^{-5} cm^2/s, while the largest intra-NAPL diffusion coefficient (D_{ii}) is ~10^{-7} cm^2/s suggesting that diffusion in water was not limiting for the systems we considered.

To estimate the activity coefficients using the UNIFAC method, the identified components and bulk portion (Table 1) were separated into multiple functional groups. Since it is not possible to identify the functional groups in the bulk portion, experimental activity coefficients for the nine detected components were estimated by dividing the experimental equilibrium concentrations by the ideal concentrations determined by modified Raoult's Law (Table 2). The initial experimental and UNIFAC activity coefficients were similar (Table 1) assuming that the bulk portion contains an equal number (9) of all the individual functional groups which represents the identified 19 components.

The sphere radius was discretized into 0.005 cm control volumes, and a time step increment of 0.1 day was adopted. A mesh convergence test indicated that the NAPL concentration generated using finer mesh increments and time steps varied by < 1%. The duration of all simulations performed was 1000 days which was deemed sufficient to observe changes in intra-NAPL diffusional flux and composition.

3.3 RESULTS AND DISCUSSION

3.3.1 Medium Viscous NAPL Used in the Experiment Investigation

The temporal dissolved phase concentration behavior of the two most predominant components in the medium viscous NAPL ($\eta = 1.2$ g/(cm s)) are presented on Figure 4 (see Figure SM-2(a) for the other components). After 1000 days of exposure to

water the concentration of naphthalene and 2-methylnaphthalene reached ~0.85 and ~0.38 mg/L, respectively. These values are

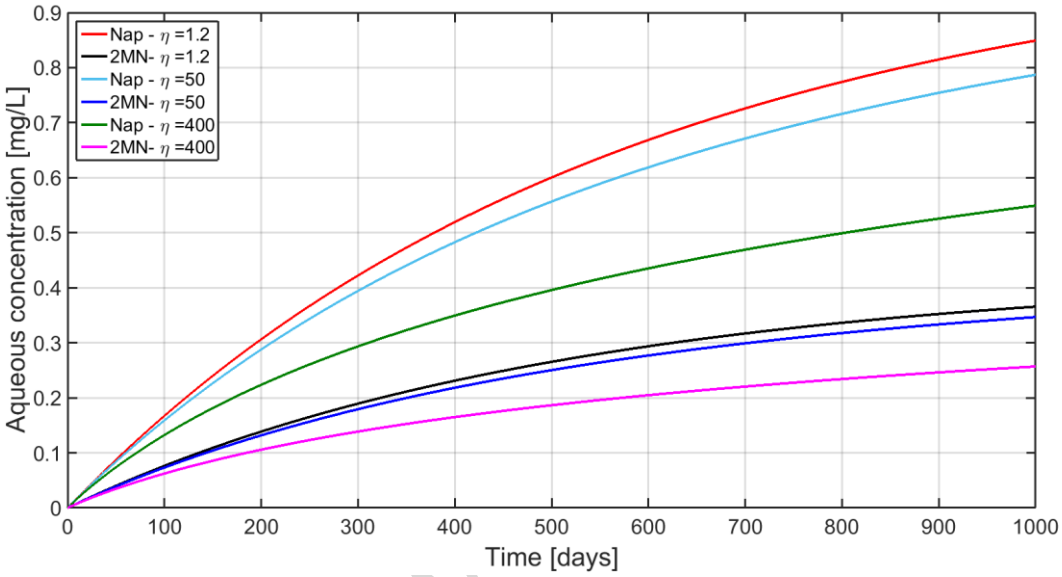

Figure 4: Aqueous concentration of naphthalene (Nap) and 2-methylnaphthalene (2MN) for the simulated medium ($\eta = 1.2$ g/(cm s)), high ($\eta = 50$ g/(cm s)), and very-high ($\eta = 400$ g/(cm s)) initial NAPL viscosities.

proportional to their initial NAPL mole fraction and aqueous solubility values (Table 1). Although phenanthrene also had one of the largest initial NAPL mole fraction values, its lower solubility resulted in a final aqueous concentration that was < 0.05 mg/L. The final (after 1000 days) radial concentration of NAPL components was homogeneous (see Figures 5 and SM-3) suggesting that mass transfer at the interface was not restricted due to intra-NAPL diffusion limitations. The ratio of the final to initial NAPL concentrations are shown in Figure 6, and indicate, as expected, that the concentration of the more soluble components such as BTEX, naphthalene, and 2-methylnaphthalene were depleted while the concentrations of the less soluble components such as phenanthrene, pyrene, and the bulk portion were enriched. After 1000 days, the viscosity of the NAPL is ~ 3 times higher than its initial value (Figure 7) and is attributed to the enrichment of the bulk portion which is composed of higher viscous and insoluble components.

While the initial main intra-NAPL diffusion coefficients (diagonal values) were ~$1x10^{-7}$ cm^2/s (Figure SM.4) the final values decreased an order of magnitude to ~$3.5x10^{-8}$ cm^2/s as a result of the changes that occurred within the NAPL body. Naphthalene which is present at the largest concentration has the highest main diffusion coefficient value. Benzene which has the lowest molecular weight has the second highest main diffusion coefficient value. Toluene, xylene, and ethylbenzene also have high main diffusion coefficient values due to their low molecular weight, density, and viscosity values. 1-methylnaphthalene, 2-methylnaphthalene, and indene after naphthalene have the largest main diffusion coefficient values amongst the PAHs. The large main diffusion coefficients for 1-methylnaphthalene and 2-methylnaphthalene are attributed to their high NAPL concentrations, while for indene its large main diffusion coefficient is due to its lower molecular weight compared to the other PAHs. Chrysene with the largest molecular weight, density, and viscosity values has the lowest diffusion coefficient value. The ratios of the final to initial main intra-NAPL diffusion coefficients (Figure SM.5) indicate that the main diffusion coefficient for naphthalene decreased more than the other components since the concentration of naphthalene was the most depleted (Figure SM.3). In contrast, the

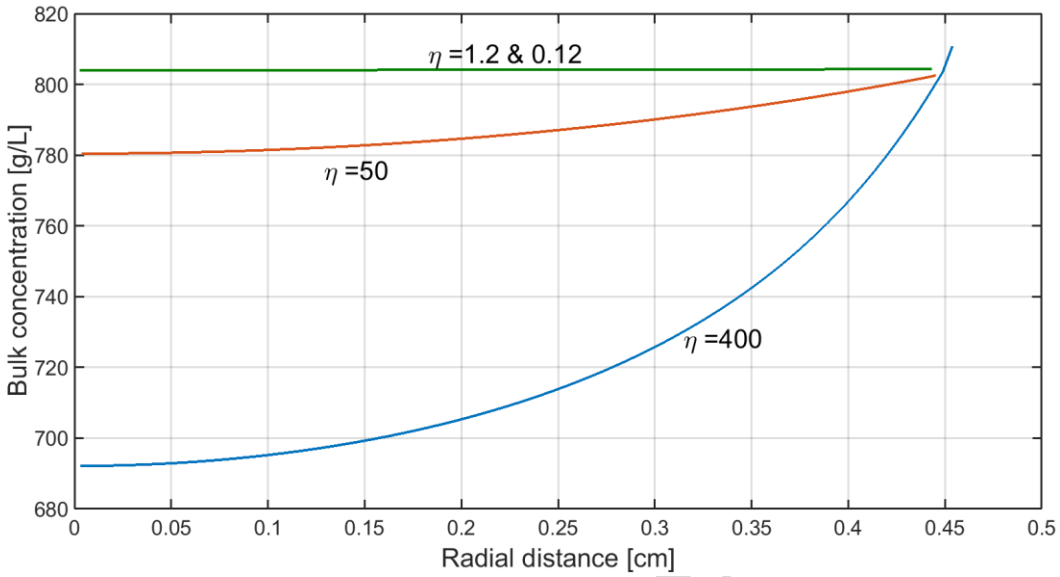

main diffusion coefficient for phenanthrene decreased the least as a result of its increase in NAPL concentration at 1000 days (Figure 6). The initial off-diagonal diffusion coefficient values were between one to three orders of magnitude lower than the main diffusion coefficient values (Table SM-3).

Figure 5: Radial bulk concentration profiles for the four initial NAPL viscosities simulated at 1000 days.

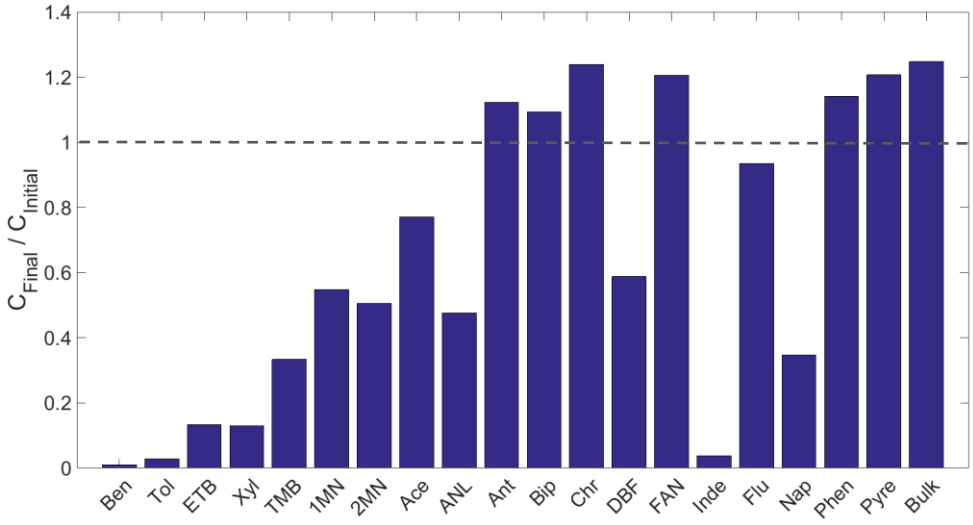

Figure 6: Ratio of final (at 1000 days) to initial component concentration within the medium viscous NAPL. From left to right: BTEX, TMB, PAHs in alphabetical order, and the bulk portion.

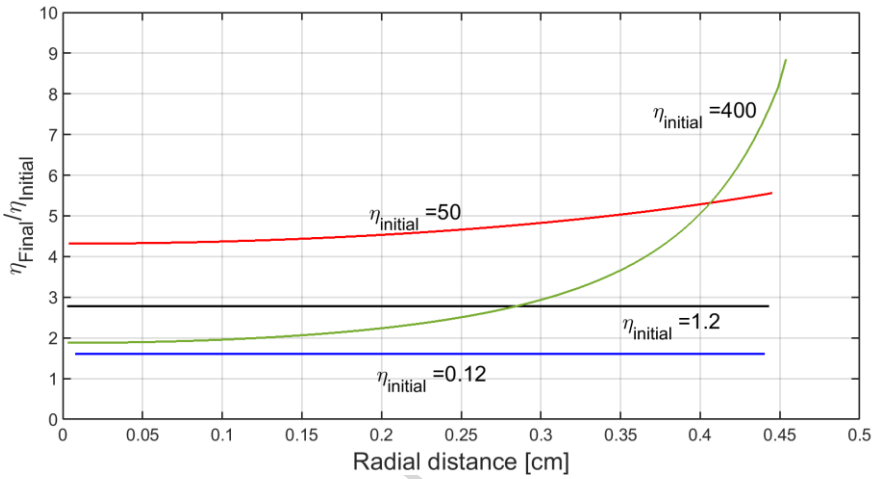

Figure 7: Ratio of final (at 1000 days) to initial viscosity as a function of radial distance from the centre of the NAPL body for the four initial NAPL viscosities investigated.

The main intra-NAPL diffusion coefficient values are not of the same order of magnitude as those reported by others. For example, Ortiz et al. (1999) reported that the diffusion coefficients for naphthalene, phenanthrene, and pyrene within transmission oils (viscosity of 8 - 14 g/(cm s)) were in the range of 10^{-9} to 10^{-12} cm^2/s after being exposed to water for ~1 year. Wehrer et al. (2013a) also reported that diffusion coefficients for some PAHs (e.g., naphthalene, acenaphthene, and pyrene) in MGP residuals were in the range of 10^{-10} to 10^{-18} cm^2/s. This difference can be attributed to the experimental conditions (i.e., NAPL composition, higher viscosity, and larger mass transfer rate coefficient) used compared to the experiments performed in this study.

For a spherical blob composed of a medium viscosity NAPL and with mass < 50 g exposed to water, diffusion-limited mass transfer and interfacial depletion of organic components due to intra-NAPL diffusion are not expected to occur. Concentration gradients at the interface due to dissolution can be quickly compensated by diffusional transport to the interface and the NAPL concentration remains homogenous. A sensitivity analyses was conducted to explore potential conditions when intra-NAPL diffusion limitations would arise for this medium viscosity NAPL. The results of this analysis indicated that when the mass transfer rate coefficient is increased to > 15 cm/day, intra-NAPL concentration gradients can be established and intra-NAPL diffusion limitations will occur. Hence, for the medium viscous NAPL due to the relatively large intra-NAPL diffusion coefficients when K values are <15 cm/day mass, mass transfer is governed by the stagnant film at the NAPL-water interface and the NAPL remains homogeneous. For K values >15 cm/day, mass transfer is governed by intra-NAPL diffusion.

3.3.2 Influence of Viscosity

Similar to the medium viscous NAPL, no concentration gradient was established in the low viscous NAPL (η=0.12 g/(cm s)) and mass transfer was not restricted. Hence,

the simulated aqueous (Figures 4 and SM.2(a)) and radial NAPL concentrations (Figures 5 and SM.3) for the low viscous NAPL are essentially identical to those obtained for the medium viscous NAPL. A sensitivity analyses indicated that when the mass transfer rate coefficient (Eq.9) was increased to > 180 cm/day, a slight intra-NAPL concentration gradients were established for naphthalene (4.0 g/L/cm) and phenanthrene (1.1 g/L/cm) in the low viscous NAPL. Mukherji et al. (1997) determined that this magnitude of mass transfer coefficient is possible under non-static conditions without sediment for a well-mixed NAPL and aqueous phase. Thus the threshold of the mass transfer rate coefficient which can result in interfacial depletion of the more soluble compounds was estimated to be 15 and 180 cm/day for the NAPL viscosities of 1.2 and 0.12 g/(cm s), respectively, indicating that a combination of NAPL properties (i.e., viscosity) and interphase mass transfer rate can result in internal diffusion limitations. It is potentially possible that in some situations increasing the mass transfer rate may result in intra-NAPL diffusion limitations and thus restrict mass transfer and impact dissolution. For example, remediation methods such as pump-and-treat systems increase groundwater flow rate and hence the mass transfer rate, and can thus restrict internal diffusion and enhance mass transfer limitations.

For the low viscous NAPL, the initial main intra-NAPL diffusion coefficients were one order of magnitude higher (~0.9×10^{-6} cm/s) compared to those determined for the medium viscous NAPL. These initial main intra-NAPL diffusion coefficients are of the same order as the self-diffusion coefficients (Eq. 13 and Table SM.2), and thus the presence of other organic components within this low viscous NAPL does not restrict internal diffusional flux. This condition is similar to organic mixtures composed of miscible organic components which are liquids at ambient temperature (similar to the organic mixtures investigated by Kett and Anderson (1969b) and Brahma & Harmon (2003)) where intra-NAPL diffusion coefficients of the order of the self-diffusion coefficients can be expected.

The simulated aqueous concentrations for the high viscous NAPL (η = 50 g/(cm.s)) at 1000 days are lower than the results from the medium viscous NAPL (Figures 4 and SM.2(b)). While concentration gradients are established within the high viscous NAPL (Figures 8(a) and SM.6), the internal diffusional flux does not significantly limit dissolution. The simulated NAPL concentration of the bulk portion (Figure 5) and

lower solubility components (i.e., phenanthrene, pyrene, chrysene, fluoranthene) increased at the interface after 1000 days while the higher soluble components were depleted. The estimated initial main intra-NAPL diffusion coefficients for the high viscous NAPL are of the order of 2.5×10^{-9} cm^2/s, and the initial off-diagonal diffusion coefficient values are one to three orders of magnitude lower. The main intra-NAPL diffusion coefficients are 40 times smaller than those determined for the medium viscous NAPL and these smaller values resulted in concentration gradients within the NAPL body. The main intra-NAPL diffusion coefficients after being exposed to water for 1000 days were five times smaller than the initial values and on the order of 5.5×10^{-10} cm^2/s. This decrease can be attributed to the depletion of the more soluble and lower viscous components (e.g., BTEX) indicating that over the time internal diffusion limitations can become more significant. The final viscosity of the high viscous NAPL is ~5 times larger than the initial value (Figure 7). The abundance of the bulk portion and lower solubility components at the interface causes the viscosity at the NAPL/water interface to be ~20 % larger than the viscosity at the centre of the NAPL body (Figure 7).

The simulated radial concentration of components within the very-high viscous NAPL (η = 400 g/(cm s)) at 1000 days for the most predominant components are shown in Figure 8 (b) (see Figure SM.6 for other components). The changes in the NAPL composition are similar to the high viscous NAPL (Figure 8 (a)) with the higher soluble components depleted at the interface. The bulk portion (Figure 5) as well as low solubility components (i.e., phenanthrene and pyrene) accumulate at the interface. However, in contrast to the high viscous NAPL, concentration gradients are more pronounced. For example, the naphthalene concentration at the interface of the very-high viscous NAPL is ~25% of the concentration in the core of the NAPL body (Figure 8(b)).

Figure 9 shows the temporal variations of the mole fractions at the interface and within the entire very-high viscous NAPL body for the most predominant components (see Figure SM.7 for other components). While naphthalene is the most dominant component within the entire very-high viscous NAPL body over the 1000-day simulation period, the interfacial naphthalene mole fraction after ~350 days decreased to less than the interfacial mole fraction of phenanthrene. As a result of the accumulation of the bulk portion and lower soluble components (e.g.,

phenanthrene and pyrene) at the interface, the aqueous equilibrium concentrations (Eq.5) and mass transfer of the higher soluble components decreased. While the simulated aqueous concentrations of the lower soluble components (e.g., fluoranthene, chrysene, and pyrene) for the very high-viscous NAPL are 15 to 30 % higher compared to those estimated for the medium viscous NAPL at 1000 days, the aqueous concentration of the remainder of the components are 15 to 40 % lower (Figures 4 and SM.2(c)). After 1000 days, the shrinkage (initial radius minus final radius) of the NAPL body for the high and very-high viscous NAPLs are 95 and 70 % of the shrinkage determined for the medium viscous NAPL body, respectively. Figure 10 indicates the temporal variation of the quantified mass loss for the different NAPL viscosities investigated. The total quantified mass loss for the low, medium, and high viscous NAPLs is ~45% after 1000 days, and for the vey-high viscous NAPL is < 33%. This difference highlights the impact that intra-NAPL diffusion has on mass transfer and hence total mass loss.

The estimated initial main intra-NAPL diffusion coefficients for the very-high viscous NAPL are 300 times smaller (~$3x10^{-10}$ cm^2/s) than those estimated for the medium viscous NAPL. The radial main intra-NAPL diffusion coefficients after being exposed to water for 1000 days (Figure 11) decreased compared to the initial values. At the NAPL/water interface all of the main intra-NAPL diffusion coefficients are ~4 times smaller than within the core of the NAPL body as a result of the depletion of lower viscous components. The abundance of the bulk portion and higher viscous components at the interface causes the viscosity at the NAPL/water interface to increase ~4.5 times relative to the centre of the NAPL body (Figure 7) at 1000 days, and ~9 times compared to the initial viscosity.

(a)

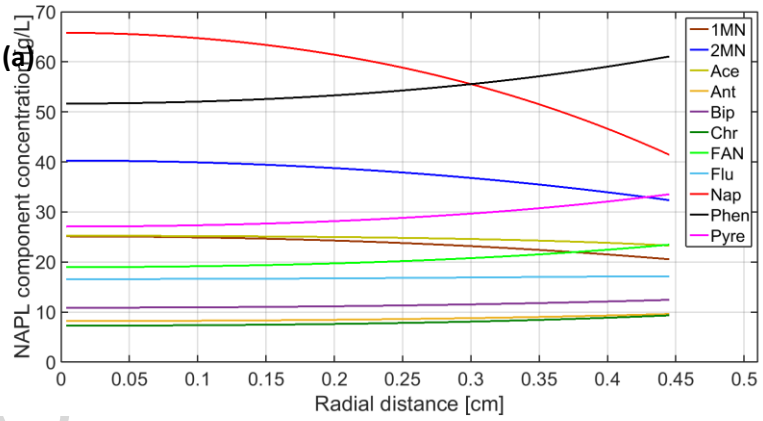

(b)

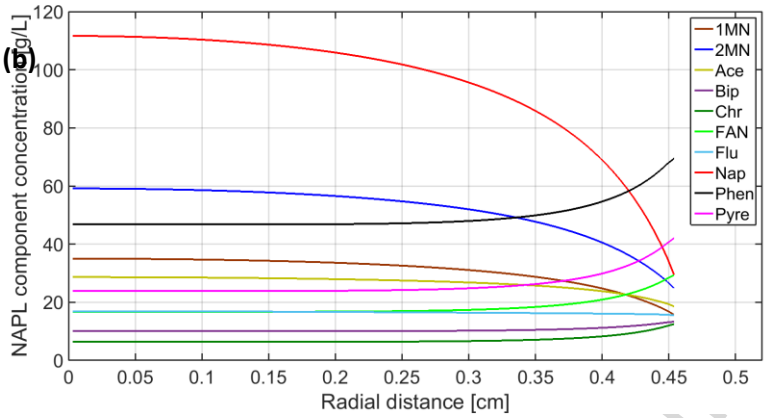

Figure 8: Simulated radial composition of the most predominant NAPL components at 1000 days for (a) the high viscous NAPL ($\eta_{initial}$ = 50 g/(cm s)), and (b) the very-high viscous NAPL ($\eta_{initial}$ = 400 g/(cm s)).

(a)

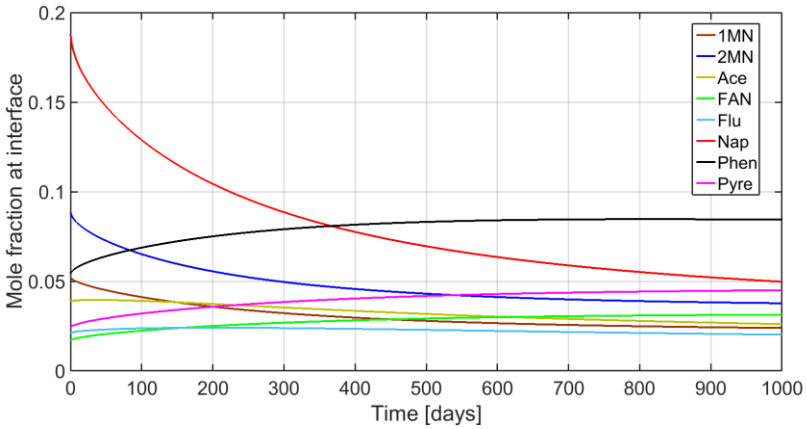

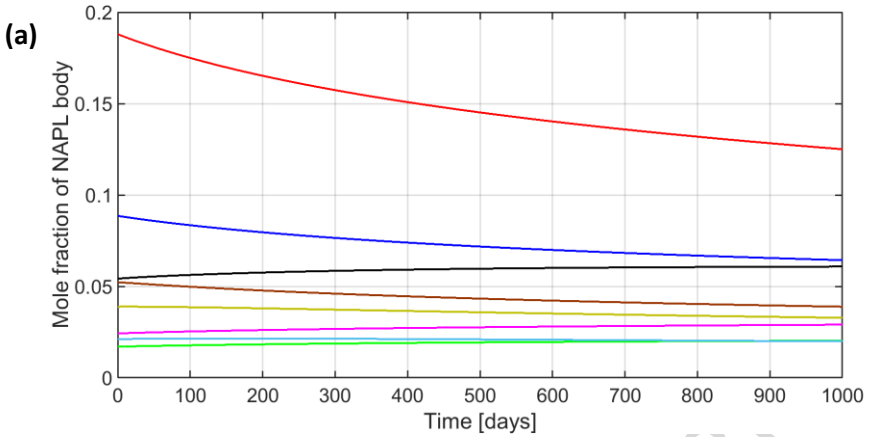

Figure 9: Temporal variation of (a) the mole fraction at the aqueous/NAPL interface, and (b) the mole fraction of the entire NAPL body for the very-high viscous NAPL ($\eta_{initial}$ = 400 g/(cm s)).

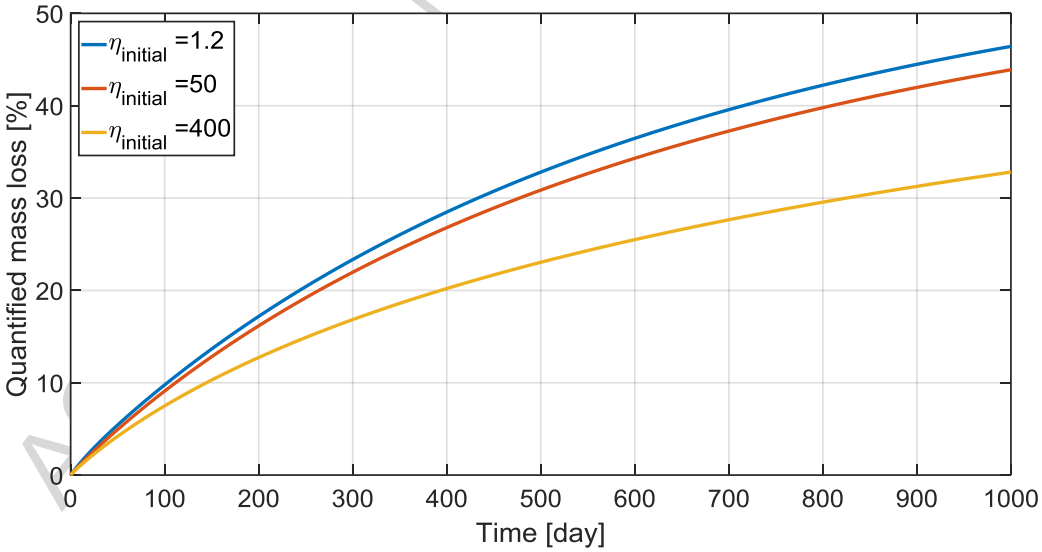

Figure 10: Temporal variation of the quantified mass loss for different initial NAPL viscosities investigated.

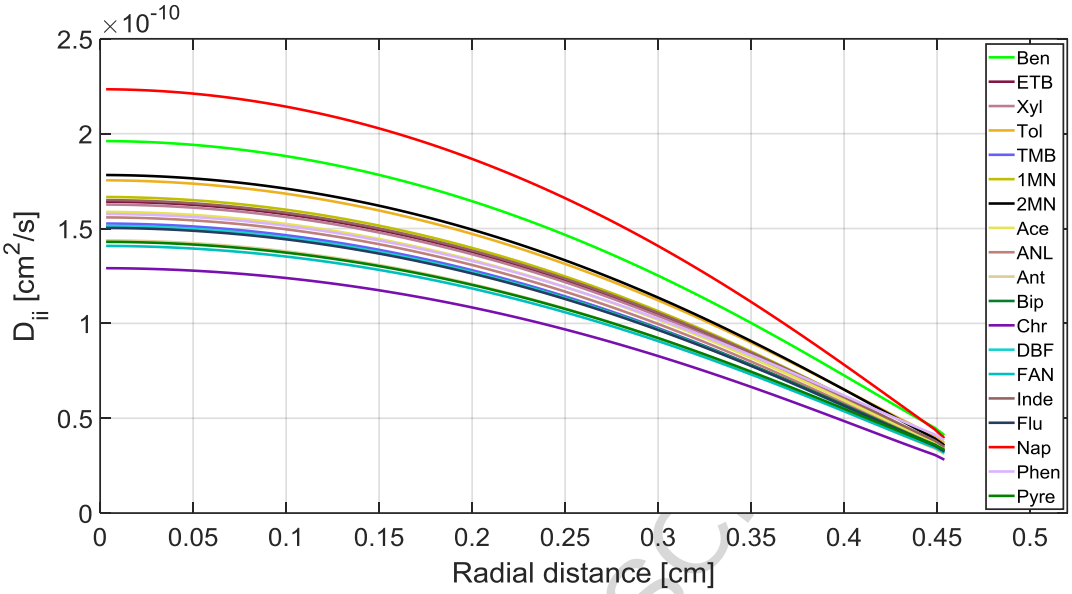

Figure 11: Radial distribution of the main intra-NAPL diffusion coefficients for the very-high viscous NAPL ($\eta_{initial}$ = 400 g/(cm s)) at 1000 days.

4.0 SUMMARY

A comprehensive experimental and computational study was performed to investigate the role of intra-NAPL diffusion on the mass transfer between multi-component NAPLs and water, and to identify some of the controlling situations where this process should be considered. A series of static experiments was conducted to investigate diffusion-controlled dissolution of organic components from former MGP residuals. The results indicated that under the diffusion-controlled mass transfer conditions established, the estimated mass transfer rate coefficients were lower than typical mass transfer rate coefficients determined under continuous mixed conditions. Although, no overall trend was observed between the mass transfer rate coefficients for the various organic compounds identified, an inverse dependency between the mass transfer rate coefficient and molecular weight was clear but different for BTEX and some PAHs compounds suggesting that the intra-NAPL diffusion behavior of these two organic compound classes are different.

To examine the role of intra-NAPL diffusion on NAPL-water mass transfer, we simulated a physical system where an isolated spherical NAPL blob was surrounded by a finite volume of water. In this system, the initial composition of the NAPL blob was assumed to be homogeneous, and the total surface area was available for mass transfer. The experimental data set assembled was used to inform the model parameters so that representative physical and chemical properties were used. The results indicated that molecular weight and concentration of each component are the most important parameters affecting intra-NAPL diffusion coefficients. Four NAPLs with different viscosities but the same quantified mass were simulated. For a spherical NAPL body of < 50 g under static conditions, the combination of NAPL properties and interphase mass transfer rate can result in internal diffusion limitations. If the main intra-NAPL diffusion coefficients are in the range of the self-diffusion coefficients (10^{-5} to 10^{-6} cm^2/s), intra-NAPL diffusion is not limiting since component concentration gradients within the NAPL cannot be established except when high mass transfer rates are present (>180 cm/day). In the case of complex and highly viscous NAPLs, smaller intra-NAPL diffusion coefficients are expected and even the low range of mass transfer rates can result in the interfacial depletion of the more soluble compounds and diffusion-limited dissolution.

In this study we investigated the effect of just one phenomenon (intra-NAPL diffusion) which can result in restricted interfacial mass transfer; however, other phenomena such as inter-molecular interactions and biofilm formation can influence NAPL-water mass transfer. For example, Mukherji and Weber (1998) reported that interfacial biofilm formation limited NAPL-water mass transfer. Possible compositional changes, solidification, and precipitation (Peters et al. 1999) as well as interfacial weak bonds between organic components and water (Nelson et al., 1996) can also result in diffusional limitations.

The diffusion-based numerical model developed in this study provides a suitable platform to capture the temporal and spatial compositional changes within complex NAPLs. The simulation results showed that intra-NAPL diffusion can significantly affect mass transfer and dissolved phase concentrations, and that increasing the NAPL-water mass transfer rate may result in intra-NAPL diffusion limitation and restricted dissolution. As a result, consideration should be given to the role of intra-NAPL diffusion in risk assessment evaluations, and during the design and

implementation of remediation strategies. Specifically, when high viscous NAPLs are present or when large mass transfer rate coefficients are expected, intra-NAPL diffusion can restrict mass transfer and thus increase the remediation timeframe of some treatment technologies.

5.0 ACKNOWLEDGEMENTS

Financial support for this investigation was provided by a Natural Sciences and Engineering Research Council (NSERC) of Canada Collaborative Research and Development Grant (N.R. Thomson). We thank Andrew Brey (Geosyntec Consultants) and Chris Gasinski (TECO Peoples Gas) for providing us with the former MGP NAPL samples used in this study.

6.0 REFERENCES

Albright, J. G., & Mills, R. (1965). A Study of Diffusion in the Ternary System, Labeled Urea-Urea-Water at 25 °C by Measurements of the Intradiffusion Coefficients of Urea. *The Journal of Physical Chemistry*, *69*(9), 3120–3126. http://doi.org/10.1021/j100893a052

Alshafie, M., & Ghoshal, S. (2004). The role of interfacial films in the mass transfer of naphthalene from creosotes to water. *Journal of Contaminant Hydrology*, *74*(1–4), 283–298. http://doi.org/10.1016/j.jconhyd.2004.03.004

Banerjee, S. (1984). Solubility of organic mixtures in water. *Environmental Science & Technology*, *18*(8), 587–91. http://doi.org/10.1021/es00126a004

Barranco, F. T., & Dawson, H. E. (1999). Influence of aqueous pH on the interfacial properties of coal tar. *Environmental Science and Technology*, *33*(10), 1598–1603. http://doi.org/10.1021/es980196r

Birak, P. S., & Miller, C. T. (2009). Dense non-aqueous phase liquids at former manufactured gas plants: challenges to modeling and remediation. *Journal of Contaminant Hydrology*, *105*(3–4), 81–98. http://doi.org/10.1016/j.jconhyd.2008.12.001

Bird, R. B., Stewart, W. E., & Lightfoot, E. N. (2002). *Transport Phenomena*. New York: John Wiley & Sons, Inc.

Brahma, P. P., & Harmon, T. C. (2003). The effect of multicomponent diffusion on NAPL dissolution from spherical ternary mixtures. *Journal of Contaminant Hydrology*, *67*, 43–60. http://doi.org/10.1016/S0169-7722(03)00087-1

Brown, C. E., & Neustadter, E. L. (1980). The wettability of oil/water/silica systems with reference to oil recovery. *Journal of Canadian Petroleum Technology*, *19*(3), 100–109. http://doi.org/10.2118/80-03-06

Brown, D. G., Knightes, C. D., & Peters, C. A. (1999). Risk Assessment for Polycyclic Aromatic Hydrocarbon NAPLs Using Component Fractions. *Environ. Sci. Technol.*, *33*(24), 4357–4363.

Crank, J. (1975). *The mathematics of diffusion*. *Annals of Nuclear Energy*. Oxford university Press. http://doi.org/10.1016/0306-4549(77)90072-X

Crank, J. (1984). *Free and moving boundary problems*. Oxford university Press.

Crank, J., & Gupta, R. S. (1972). A method for solving moving boundary problems in heat flow using cubic splines or polynomials. *IMA Journal of Applied Mathematics*, *10*(3), 296–304. Retrieved from http://hdl.handle.net/2438/2288

Cussler, E. L. (1997). *Diffusion Mass Transfer in Fluid Systems* (Second edi). Cambridge University Press.

Eberhardt, C., & Grathwohl, P. (2002). Time scales of organic contaminant dissolution from complex source zones: coal tar pools vs. blobs. *Journal of*

Contaminant Hydrology, *59*(1–2), 45–66.

Ghoshal, S., Pasion, C., & Alshafie, M. (2004). Reduction of Benzene and Naphthalene Mass Transfer from Crude Oils by Aging-Induced Interfacial Films. *Environmental Science and Technology*, *38*(7), 2102–2110. http://doi.org/10.1021/es034832j

Ghoshal, S., Ramaswami, A., & Luthy, R. G. (1996). Biodegradation of naphthalene from coal tar and heptamethylnonane in mixed batch systems. *Environmental Science and Technology*, *30*(4), 1282–1291. http://doi.org/10.1021/es950494d

Grunberg, L., & Nissan, A. H. (1949). Mixture Law for Viscosity. *Nature*, *164*, 799–800.

Hartley, G. S., & Crank, J. (1949). Some fundamental definitions and concepts in diffusion processes. *Transactions of the Faraday Society*, *45*, 801–818. http://doi.org/10.1039/TF9494500801

Heyse, E., Augustijn, D., Rao, P. S. C., & Delfino, J. J. (2002). Nonaqueous Phase Liquid Dissolution and Soil Organic Matter Sorption in Porous Media: Review of System Similarities. *Critical Reviews in Environmental Science and Technology*, *32*(4), 337–397. http://doi.org/10.1080/10643380290813471

Holman, H.-Y. N., & Javandel, I. (1996). Evaluation of Transient Dissolution of Slightly Water-Soluble Compounds From a Light Nonaqueous Phase Liquid Pool. *Water Resources Research*, *32*(4), 915–923. http://doi.org/10.1029/96WR00075

Houghton, G. (1964). Cubic Cell Model for Self-Diffusion in Liquids. *The Journal of Chemical Physics*, *40*(6), 1628. http://doi.org/10.1063/1.1725371

Hunt, J. R., Sitar, N., & Udell, K. S. (1988). Nonaqueous phase liquid transport and cleanup: 2. Experimental studies. *Water Resour. Res.*, *24*(8), 1259–1269. http://doi.org/10.1029/WR024i008p01259

Jada, A., & Salou, M. (2002). Effects of the asphaltene and resin contents of the bitumens on the water-bitumen interface properties. *Journal of Petroleum Science and Engineering*, *33*(1–3), 185–193. http://doi.org/10.1016/S0920-4105(01)00185-1

Kett, T. K., & Anderson, D. K. (1969a). Multicomponent Diffusion in Nonassociating, Nonelectrolyte Solutions. *J. Phys. Chem.*, *73*, 1262–1267.

Kett, T. K., & Anderson, D. K. (1969b). Ternary isothermal diffusion and the validity of the Onsager reciprocal relations in nonassociating systems. *J. Phys. Chem.*, *73*(8), 1268–1274.

Khachikian, C., & Harmon, T. C. (2000). Nonaqueous Phase Liquid Dissolution in Porous Media : Current State of Knowledge and Research Needs. *Transport in Porous Media*, *38*(5), 3–28.

Leahy-Dios, A., & Firoozabadi, A. (2007). Unified model for nonideal multicomponent molecular diffsuion coefficients. *AIChE Journal*, *53*, 2932–2939.

http://doi.org/10.1002/aic

Lee, L. S., Rao, P. S. C., & Okuda, I. (1992). Equilibrium partitioning of polycyclic aromatic hydrocarbon from coal tars into water. *Environ. Sci. Technol.*, *26*(11), 2110–2115.

Lekmine, G., Bastow, T. P., Johnston, C. D., & Davis, G. B. (2014). Dissolution of multi-component LNAPL gasolines: the effects of weathering and composition. *Journal of Contaminant Hydrology*, *160*, 1–11. http://doi.org/10.1016/j.jconhyd.2014.02.003

Lide, D. R. (1999). *CRC handbook of physics and chemistry*.

Liu, L., Endo, S., Eberhardt, C., Grathwohl, P., & Schmidt, T. C. (2009). Partition Behavior of Polycyclic Aromatic Hydrocarbons Between Aged Coal Tar and Water. *Environmental Toxicology and Chemistry*, *28*(8), 1578–1584.

Luthy, R. G., Dzombak, D. A., Peters, C. A., Roy, S. B., Ramaswami, A., Nakles, D. V., & Nott, B. R. (1994). Remediating Tar-Contaminated Soils at Manufactured Gas Plant Sites: Technological Challenges. *Environ. Sci. Technol.*, *28*(6), 266A–276A.

Luthy, R. G., Ramaswaml, A., Ghoshal, S., & Merkelt, W. (1993). Interfacial Films in Coal Tar Nonaqueous-Phase Liquid-Water Systems. *Environ. Sci. Technol.*, *27*(13), 2914–2918.

Mackay, D., Shiu, W.-Y., Ma, K.-C., & Lee, S. C. (2006). *Handbook of Physical-Chemical Properties and Environmental Fate for Organic Chemicals, Second Edition*. CRC Press, Talor & Francis Group.

Mahjoub, B., Jayr, E., Bayard, R., & Gourdon, R. (2000). Phase partition of organic pollutants between coal tar and water under variable experimental conditions. *Water Research*, *34*(14), 3551–3560. http://doi.org/10.1016/S0043-1354(00)00100-7

Mercer, J. W., & Cohen, R. M. (1990). A review of immiscible fluids in the subsurface: Properties, models, characterization and remediation. *J. Contaminant Hydrology*, *6*, 107–163.

Miller, C. T., Poirier-Mcneill, M. M., & Mayer, A. S. (1990). Dissolution of trapped nonaqueous phase liquids: mass transfer characteristics. *Water Resources Research*, *26*, 2783–2796.

Miller, M. M., Waslk, S. P., Huang, G.-L., Shiu, W.-Y., & Mackay, D. (1985). Relationships between Octanol-Water Partition Coefficient and Aqueous Solubility. *Environ. Sci. Technol.*, *19*(6), 522–529.

Mobile, M., Widdowson, M., Stewart, L., Nyman, J., Deeb, R., Kavanaugh, M., … Gallagher, D. (2016). In-situ determination of field-scale NAPL mass transfer coefficients : Performance , simulation and analysis. *Journal of Contaminant Hydrology*, *187*, 31–46. http://doi.org/10.1016/j.jconhyd.2016.01.010

Mukherji, S., Peters, C. a., & Weber, W. J. (1997). Mass Transfer of Polynuclear Aromatic Hydrocarbons from Complex DNAPL Mixtures. *Environmental Science*

& Technology, *31*(2), 416–423. http://doi.org/10.1021/es960227n

Mukherji, S., & Weber, W. J. (1998). Mass Transfer Effects on Microbial Uptake of Naphthalene from Complex NAPLs Mass Transfer Effects on Microbial Uptake of Naphthalene from Complex NAPLs. *Biotechnol. Bioeng.*, *60*, 750–760.

Nelson, E. C., Ghoshal, S., Edwards, J. C., Marsh, G. X., & Luthy, R. G. (1996). Chemical Characterization of Coal Tar - Water Interfacial Films. *Environ. Sci. Technol.*, *30*(3), 1014–1022.

Ortiz, E., Kraatz, M., & Luthy, R. G. (1999). Organic Phase Resistance to Dissolution of Polycyclic Aromatic Hydrocarbon Compounds. *Environ. Sci. Technol.*, *33*(2), 235–242.

Peters, C. A., Knightes, C. D., & Brown, D. G. (1999). Long-Term Composition Dynamics of PAH-Containing NAPLs and Implications for Risk Assessment. *Environ. Sci. Technol.*, (609), 4499–4507.

Peters, C. A., Mukherji, S., Knightes, C. D., & Weber, W. (1997). Phase Stability of Multicomponent NAPLs Containing PAHs. *Environ. Sci. Technol.*, *31*(9), 2540–2546.

Peters, C. A., Wammer, K. H., & Knightes, Christopher, D. (2000). Multicomponent NAPL Solidification Thermodynamics. *Transport in Porous Media*, *38*, 57–77.

Poling, B. E., Prausnitz, J. M., & O'Connell, J. P. (2001). *Properties of Gases and Liquids, Fifth Edition*. McGraw-Hill Education. Retrieved from http://accessengineeringlibrary.com/browse/properties-of-gases-and-liquids-fifth-edition#fullDetails

Powers, E., Abriola, M., & Weber, J. (1992). An Experimental Investigation of Nonaqueous Phase Liquid Dissolution in Saturated Subsurface Systems â€™ Steady State Mass Transfer Rates. *Water Resources Research*, *28*(10), 2691–2705.

Powers, S. E., Anckner, W. H., & Seacord, T. F. (1996). Wettability of NAPL-Contaminated sands. *J. Environ. Eng.*, *122*(1), 889–896.

Powers, S. E., Nambi, I. M., & Curry Jr., G. W. (1998). Non-aqueous phase liquid dissolution in heterogeneous systems : Mechanisms and a local equilibrium modeling approach. *Water Resources Research*, *34*(12), 3293–3302.

Seagren, E. a., Rittmann, B. E., & Valocchi, A. J. (1999). An experimental investigation of NAPL pool dissolution enhancement by flushing. *Journal of Contaminant Hydrology*, *37*(1–2), 111–137. http://doi.org/10.1016/S0169-7722(98)00157-0

Seagren, E. a, Rittmann, B. E., & Valocchi, A. J. (1993). Quantitative evaluation of flushing and biodegradation for enhancing in situ dissolution of nonaqueous-phase liquids. *Journal of Contaminant Hydrology*, *12*(1–2), 103–132. http://doi.org/10.1016/0169-7722(93)90017-M

Soga, K., Page, J. W. E., & Illangasekare, T. H. (2004). A review of NAPL source

zone remediation efficiency and the mass flux approach. *Journal of Hazardous Materials*, *110*(1–3), 13–27. http://doi.org/10.1016/j.jhazmat.2004.02.034

Strassner, J. E. (1968). Effect of pH on Interfacial Films and Stability of Crude Oil-Water Emulsions. *Journal of Petroleum Technology*, *20*(3), 303–312. http://doi.org/10.2118/1939-PA

Thomson, N. R., Fraser, M. J., Lamarche, C., Barker, J. F., & Forsey, S. P. (2008). Rebound of a coal tar creosote plume following partial source zone treatment with permanganate. *Journal of Contaminant Hydrology, 102(1–2), 154–71.*

Varadaraj, R., & Brons, C. (2012). Molecular origins of crude oil interfacial activity. part 4: Oil-water interface elasticity and crude oil asphaltene films. *Energy and Fuels*, *26*(12), 7164–7169. http://doi.org/10.1021/ef300830f

Weber, W. J., & DiGiano, J. F. A. (1995). *process dynamic in environmental systems*. John Wiley & Sons, Inc.

Wehrer, M., Mai, J., Attinger, S., & Totsche, K. U. (2013a). Kinetic control of contaminant release from NAPLs--information potential of concentration time profiles. *Environmental Pollution*, *179*, 301–14. http://doi.org/10.1016/j.envpol.2013.04.029

Wehrer, M., Rennert, T., & Totsche, K. U. (2013b). Kinetic control of contaminant release from NAPLs--experimental evidence. *Environmental Pollution*, *179*, 315–25. http://doi.org/10.1016/j.envpol.2013.03.041

Zielinski, J. M., & Hanley, B. F. (1999). Practical friction-based approach to modeling multicomponent diffusion. *AIChE Journal*, *45*(1), 1–12. http://doi.org/10.1002/aic.690450102

Table 1: Suite of organic components detected in the former MGP NAPL used in this study along with associated properties

		Aqueous	NAPL	Mole				Density	Viscosity	$V_{boiling}$		
	Identifier	MDL	Concentration	Fraction	MW	Solubility	f^S/f^L		(Eq.11)	(Eq.14)	Initial Activity Coefficient	
Component		[µg/L]	[g/L]	[-]	[g/mol]	[mg/L]	[-]	[g/mL]	[g/(cm s)]	[cm^3/mol]	Experimental	UNIFAC
Benzene	Ben	1.11	2.84E+00	6.89E-03	78.1	1780 [1]	1 [1]	0.88	6.49E-03	77	0.42	0.25
Ethylbenzene	ETB	0.77	5.97E+00	1.07E-02	106.2	161.2 [1]	1 [1]	0.87	6.78E-03	119	0.49	0.38
Xylene(s)	Xyl	1.46	3.50E+00	6.27E-03	106	373 [1]	1 [1]	0.87	6.97E-03	119	0.41	0.40
Toluene	Tol	0.83	1.13E+00	2.34E-03	92.1	534.8 [1]	1 [1]	0.86	6.00E-03	98	0.04	0.33
Trimethylbenzene(s)	TMB	0.82	5.78E+00	9.13E-03	120.2	57.4 [1]	1 [1]	0.88	8.75E-03	140	0.45	0.47
1-Methylnaphthalene	1MN	1.31	3.92E+01	5.23E-02	142.2	28.5 [1]	1 [1]	1.02	1.63E-02	140	0.38	0.49
2-Methylnaphthalene	2MN	4.27	6.63E+01	8.85E-02	142.2	25.4 [1]	0.86 [1]	1.01	1.63E-02	140	0.21	0.49
Acenaphthene	Ace	1.83	3.16E+01	3.89E-02	154.2	3.9 [1]	0.2 [1]	1.22	3.02E-02	147	0.22	0.64
Acenaphthylene	ANL	1.53	7.89E+00	9.83E-03	154	9.8 [1]	0.22 [1]	0.90	2.05E-02	133	-	0.57
Anthracene	Ant	5.53	8.19E+00	8.72E-03	178.2	0.05 [1]	0.01 [1]	1.28	4.10E-02	161	-	0.60
Biphenyl	Bip	1.09	1.10E+01	1.35E-02	154.2	7.5 [2]	1 [3]	1.04	2.08E-02	147	-	0.45
Chrysene	Chr	5.75	6.90E+00	5.74E-03	228.2	0.002 [1]	0.0097 [1]	1.27	9.32E-02	203	-	0.86
Dibenzofuran	DBF	1.11	4.82E+00	5.44E-03	168.2	10 [2]	0.25 [4]	1.09	3.23E-02	140	-	0.55
Fluoranthene	FAN	1.81	1.81E+01	1.70E-02	202.3	0.26 [1]	0.21 [1]	1.25	7.24E-02	175	-	0.86
Indene	Inde	2.21	2.42E-01	3.95E-04	116.2	390 [1]	1 [3]	1.00	1.10E-02	112	-	0.42
Fluorene	Flu	1.88	1.85E+01	2.11E-02	166.2	2 [1]	0.16 [1]	1.20	3.64E-02	154	-	0.63
Naphthalene	Nap	2.21	1.27E+02	1.88E-01	128.2	31.7 [1]	0.3 [1]	1.03	1.32E-02	119	0.35	0.40
Phenanthrene	Phen	3.78	5.09E+01	5.42E-02	178.2	1.3 [1]	0.28 [1]	0.98	3.14E-02	161	-	0.60
Pyrene	Pyre	1.61	2.59E+01	2.43E-02	202.3	0.13 [1]	0.11 [1]	1.27	6.39E-02	175	-	0.86
Bulk	Bulk	-	6.45E+02	4.37E-01	280 [5]	2.00E-06 [5]	1.00	1.14	8.00E+00	119 [6]	-	0.73
1) From Eberhardt & Grathwohl (2002).												
2) From Thomson et al. (2008).												

3) Not available; assumed equal to unity.											
4) From Mackay et al. (2006).											
5) Assumed.											
6) Assumed similar to naphthalene.											

Table 2: Aqueous equilibrium concentration, and experimental lumped mass transfer rate coefficient (*K*), for the nine detected components present in the aqueous phase.

Aqueous Equilibrium Concentration				
	Experimental	**Ideal** [1]	**K**	
Component	**[µg/L]**		**[1/day]**	r^2
Benzene	5200	12300	0.080	0.83
Ethylbenzene	850 [2]	1720	0.042	0.98
Xylene(s)	450 [2]	1090	0.036	0.98
Toluene	50	1250	0.061	0.98
Trimethylbenzene(s)	235	524	0.062	0.94
1-Methylnaphthalene	570	1490	0.093	0.91
2-Methylnaphthalene	560	2620	0.104	0.91
Acenaphthene	170	758	0.055	0.83
Naphthalene	7000 [1]	19800	0.036	0.94
1) Assuming $\gamma = 1$ in Raoult's law (Eq.5). 2) Calibrated with a least-squares analyses framework.				

Highlights

- Inverse dependency between mass transfer rate coefficient and molecular weight
- Model developed to estimate intra-NAPL diffusion within complex NAPLs
- Molecular weight and NAPL concentration impact intra-NAPL diffusion coefficients
- NAPL composition, viscosity, and mass transfer rate can limit intra-NAPL diffusion